

Chemical Science

Accepted Manuscript



This is an *Accepted Manuscript*, which has been through the Royal Society of Chemistry peer review process and has been accepted for publication.

Accepted Manuscripts are published online shortly after acceptance, before technical editing, formatting and proof reading. Using this free service, authors can make their results available to the community, in citable form, before we publish the edited article. We will replace this *Accepted Manuscript* with the edited and formatted *Advance Article* as soon as it is available.

You can find more information about *Accepted Manuscripts* in the [Information for Authors](#).

Please note that technical editing may introduce minor changes to the text and/or graphics, which may alter content. The journal's standard [Terms & Conditions](#) and the [Ethical guidelines](#) still apply. In no event shall the Royal Society of Chemistry be held responsible for any errors or omissions in this *Accepted Manuscript* or any consequences arising from the use of any information it contains.



www.rsc.org/chemicalscience

Cite this: DOI: 10.1039/c0xx00000x

www.rsc.org/xxxxxx

ARTICLE TYPE

A mitochondrion-targeting copper complex exhibits potent cytotoxicity against cisplatin-resistant tumor cells through a multiple mechanism of action

Wen Zhou,^a Xiaoyong Wang,^{*b} Ming Hu,^a Chengcheng Zhu^a and Zijian Guo^{*a}

⁵ Received (in XXX, XXX) XthXXXXXXXXXX 20XX, Accepted Xth XXXXXXXXXXXX 20XX
DOI: 10.1039/b000000x

Copper complexes are potential anticancer drugs by virtue of their available redox properties and low toxicity. In this study, a copper(II) complex, [Cu(tpy-tp)Br₂]Br [simplified as CTB, tpy-tp = 4'-p-tolyl-(2,2':6',2''-terpyridyl)triphenylphosphonium bromide], is synthesized and characterized by X-ray crystallography and ESI-MS as a targeted anticancer agent. Triphenylphosphine (TPP) is introduced into the complex for its mitochondrion-targeting ability and lipophilic character. The uptake of CTB by tumor cells and mitochondria was determined by ICP-MS or fluorescence spectrometry. CTB is able to cross the cytoplasmic and mitochondrial membranes of tumor cells and influence the mitochondrial membrane potential more profoundly than anticancer drug cisplatin. The cytotoxicity of CTB was tested on MCF-7, HeLa, Skov-3, A549 and cisplatin-resistant A549R tumor cells by MTT assay. CTB is more cytotoxic against these cells than cisplatin; particularly, it is highly effective against cisplatin-resistant tumor cells. The interaction between CTB and DNA has been studied by spectroscopic methods and agarose gel electrophoresis. CTB strongly interacts with DNA via an intercalation stabilized by electrostatic force, and displays a significant cleavage activity towards supercoiled pBR322 DNA and cellular DNA through an oxidative mechanism. The cytotoxicity of CTB seems to result from a multiple mechanism of action, including the modification of DNA conformation, generation of reactive oxygen species, scission of DNA strands, and dissipation of mitochondrial membrane potential. Delocalized cationic property and high hydrophilicity of CTB favours its selective accumulation in cancer cells and mitochondria. This study demonstrates that copper complexes with mitochondrion-targeting function could be efficient anticancer drugs immune to the drug resistance of cisplatin.

Introduction

Platinum anticancer drugs such as cisplatin, carboplatin and oxaliplatin have been applied in cancer treatment for several decades.^{1,2,3} However, their applications are largely restricted by various side effects and intrinsic or acquired drug resistance.^{4,5} It is generally accepted that platinum drugs inhibit tumor proliferation by interfering with the DNA replication in cancer cells through coordination with DNA.⁶ Nevertheless, many tumor cells have developed diverse mechanisms to repair the DNA damages and hence evolved the resistance to these drugs.⁷ Non-platinum metal complexes such as those of ruthenium and gold may circumvent the resistance through different mechanisms of action.^{8,9} Unfortunately, these metals are unessential elements for human body and therefore may produce unexpected side effects. Copper is an essential trace element for human body, and its complexes have been extensively studied as potential anticancer agents with low general toxicity.^{10,11,12} In addition, the affinity of DNA for copper ions appears to be greater than that for other essential metal ions.¹³ The biodistribution, cellular accumulation, and cytostatic process of copper complexes seem to be different

from those of platinum complexes, which create an opportunity to overcome the tumor resistance to conventional platinum drugs.¹⁴ In many cases, the cytotoxicity of copper complexes originates from the generation of reactive oxygen species (ROS) driven by the metal.¹⁵ In sporadic examples, special ligands are used to direct the toxicity of the metal toward tumor cells;¹⁶ but ligands with properties targeting at a specific cellular organelle are rarely seen in copper complexes. Therefore, targeted copper complexes are appealing objectives in finding novel drug candidates for cancer chemotherapy.

In recent years, there is a surge in developing compounds capable of targeting mitochondria for cancer therapy because dysfunction of this organelle has been linked to both apoptosis and necrosis.^{17,18} Cancer cells often have higher plasma and mitochondrial membrane potentials ($\Delta\Psi_p$ and $\Delta\Psi_m$, negative inside) than normal cells,¹⁹ which can be exploited to selectively deliver drugs to cancer cells while spare normal cells from toxicity. Triphenylphosphine (TPP) has been used as a mitochondrion-targeting moiety to deliver toxic drugs or proteins for triggering apoptosis in cancer therapy,^{20,21,22} because it could impart a delocalized charge and lipophilic character to a

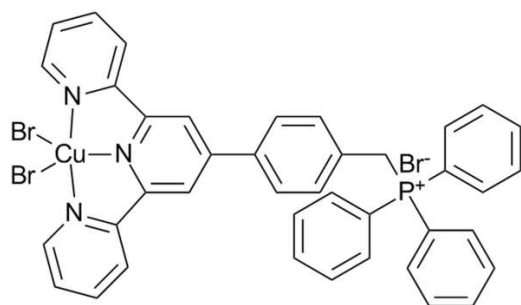


Fig. 1 Structure of $[\text{Cu}(\text{tpy-tpp})\text{Br}_2]\text{Br}$.

compound that are favourable for mitochondrial accumulation.²³ Moreover, some triphenylphosphonium salts have demonstrated antiproliferative activity in cells and animals.^{24,25} For example, a series of compounds containing a TPP moiety have shown remarkable activity in a panel of cancer cell lines and significant *in vivo* efficacy in a mouse model of human breast cancer with no apparent toxicity.²⁶ Studies on⁶⁴Cu-labeled

triphenylphosphonium cations as imaging agents have found that these copper complexes preferentially accumulate within tumor cells due to the enhanced negative $\Delta\Psi_m$ and have low uptake in the heart and muscle because of the high hydrophilicity.^{27,28}

We recently found that copper-terpyridine complexes can effectively interact with DNA and cleave it into different fragments through an oxidative mechanism.²⁹ In this study, we try to introduce TPP to the copper-terpyridine complex in order to construct a novel anticancer complex that works differently from platinum drugs (Fig. 1). We presume that TPP could enhance the intracellular accumulation of $[\text{Cu}(\text{tpy-tpp})\text{Br}_2]\text{Br}$ (CTB), especially in mitochondria, and inhibit cancer cells through DNA cleavage. To testify this assumption, the cellular and mitochondrial uptake, the cytotoxicity, the DNA binding and cleavage properties of the complex were studied by various

Results and discussion

Characterization

CTB was characterized by X-ray crystallography. Crystal parameters and structure refinement details are summarized in Table 1. Selected bond lengths and angles relevant to the copper center are listed in Table 2. Detailed crystallographic data have been deposited at the Cambridge Crystallographic Data Centre with the deposition number of CCDC 821319. These data are available for free at <http://www.ccdc.cam.ac.uk/deposit>, or from CCDC, 12 Union Road, CAMBRIDGE CB2 1EZ, UK; E-mail: deposit@ccdc.cam.ac.uk.

As the crystal structure shows (Fig. 2), there are two molecules in one minimum dissymmetric unit. The dihedral angle between two molecules is 19.56° , setting tpy of each molecule as a plane. Two molecules almost have the same direction although tpp moieties have different twist directions, suggesting that tpp could rotate freely in solution. The copper center of CTB adopts a distorted square pyramidal CuN_3Br_2 coordination geometry with tpy-tpp acting as a tridentate equatorial ligand. In CTB, three

Table 1 Crystallographic data and structure refinement parameters for CTB.

Chemical formula	$\text{C}_{40}\text{H}_{31}\text{Br}_3\text{CuN}_5\text{OP}$
Formula weight	903.92
Crystal system	Monoclinic
Space group	C2/c
a [Å]	18.610(5)
b [Å]	17.503(5)
c [Å]	46.898(5)
α [°]	90.000(5)
β [°]	98.136(5)
γ [°]	90.000(5)
V [Å ³]	15122(6)
Z	16
D_c [gcm ⁻³]	1.588
$F(000)$	7184.0
Crystal size [mm]	$0.30 \times 0.30 \times 0.10$
T [K]	298(2)
λ [Å]	0.71069
$n_{\text{ref}}, n_{\text{par}}$	13404, 883
R_1, wR_2	0.0849, 0.2537
GOF on F^2	1.121

Table 2 Selected bond lengths (Å) and angles (°) for CTB.

Bond lengths			
Cu1–N4	2.049(8)	Cu2–N1	2.026(9)
Cu1–N5	1.931(8)	Cu2–N2	1.949(8)
Cu1–N6	2.040(9)	Cu2–N3	2.065(8)
Cu1–Br3	2.6718(19)	Cu2–Br4	2.7494(19)
Cu1–Br5	2.320(2)	Cu2–Br6	2.306(2)
Bond angles			
N4–Cu1–N5	79.2(3)	N1–Cu2–N2	80.2(3)
N4–Cu1–N6	157.3(3)	N1–Cu2–N3	156.9(3)
N5–Cu1–N6	79.4(3)	N2–Cu2–N3	78.4(3)
N4–Cu1–Br5	99.0(2)	N1–Cu2–Br6	97.5(2)
N5–Cu1–Br5	160.6(3)	N2–Cu2–Br6	160.6(3)
N6–Cu1–Br5	98.6(3)	N3–Cu2–Br6	99.6(2)
N4–Cu1–Br3	90.7(2)	N1–Cu2–Br4	99.4(3)
N5–Cu1–Br3	94.3(3)	N2–Cu2–Br4	89.9(2)
N6–Cu1–Br3	98.5(3)	N3–Cu2–Br4	89.5(2)
Br3–Cu1–Br5	105.04(7)	Br4–Cu2–Br6	109.38(7)

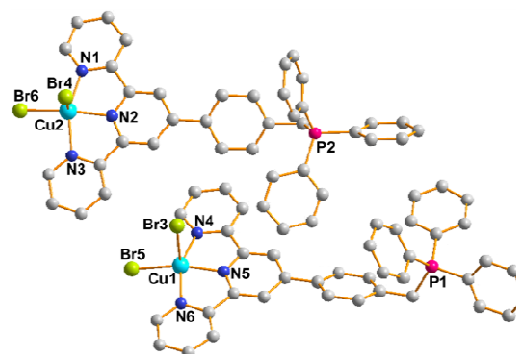


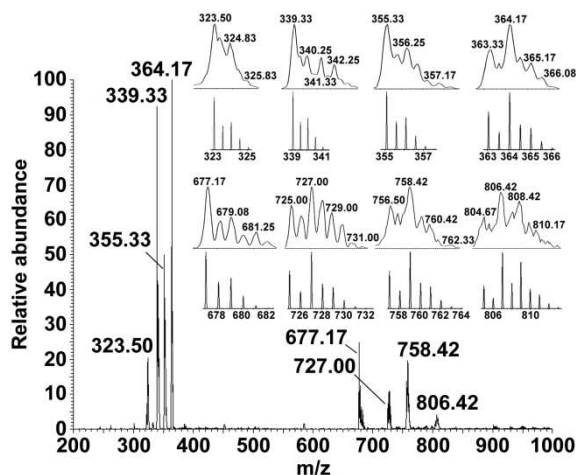
Fig. 2 Crystal structure of CTB along with the atom numbering scheme around the copper center.

nitrogen atoms from tpy (N1, N2, N3) and one bromine atom (Br6) form the basal plane, and the other bromine atom (Br4) occupies the apical position. The coordination mode of copper in CTB is almost the same as in its analogue complexes.²⁹

The stability of CTB in aqueous solution was investigated by ESI-MS. CTB shows two sets of peaks in the ESI-MS spectrum (Fig. 3): the peaks appear at m/z 323.50–364.17 could be assigned to the bivalent species; while those appear at m/z 677.17–806.42 could be assigned to the univalent species.

Table 3 Assignments of the observed peaks in the ESI-MS spectrum for CTB (see Fig. 3).

Species	Formula	Observed m/z	Calculated m/z
$[\text{CTB}-3\text{Br}-\text{H}]^{2+}$	$\text{C}_{40}\text{H}_{30}\text{CuN}_3\text{P}$	323.50–325.83	647.21/2
$[\text{CTB}-3\text{Br}-\text{H}+\text{CH}_3\text{OH}]^{2+}$	$\text{C}_{41}\text{H}_{34}\text{CuN}_3\text{PO}$	339.33–342.25	679.25/2
$[\text{CTB}-3\text{Br}-\text{H}+2\text{CH}_3\text{OH}]^{2+}$	$\text{C}_{42}\text{H}_{38}\text{CuN}_3\text{PO}_2$	355.33–357.17	711.29/2
$[\text{CTB}-2\text{Br}]^{2+}$	$\text{C}_{40}\text{H}_{31}\text{BrCuN}_3\text{P}$	363.33–366.08	728.12/2
$[\text{CTB}-3\text{Br}-2\text{H}+\text{CH}_3\text{OH}]^+$	$\text{C}_{41}\text{H}_{33}\text{CuN}_3\text{PO}$	677.17–681.25	677.17
$[\text{CTB}-2\text{Br}-\text{H}]^+$	$\text{C}_{40}\text{H}_{30}\text{BrCuN}_3\text{P}$	725.00–731.00	727.11
$[\text{CTB}-2\text{Br}-\text{H}+\text{CH}_3\text{OH}]^+$	$\text{C}_{41}\text{H}_{34}\text{BrCuN}_3\text{PO}$	756.50–762.33	759.15
$[\text{CTB}-\text{Br}]^+$	$\text{C}_{40}\text{H}_{31}\text{Br}_2\text{CuN}_3\text{P}$	804.67–810.17	806.99

**Fig. 3** ESI-MS spectrum (positive mode) and the isotopic distribution patterns of the observed peaks for CTB in water.**Table 4** The content of Cu in 10^6 different tumor cells. The calculation is based on the data of at least three independent replicates and the content of Cu in untreated cells has been subtracted.

Tumor cells	Cu content (ng)
MCF-7	114.75 ± 2.21
HeLa	48.65 ± 2.49
Skov-3	31.72 ± 0.72
A549	97.08 ± 2.27
A549R	107.52 ± 1.71

Detailed assignments for the peaks are listed in Table 3. The isotopic distribution patterns of all the observed species are consistent with the theoretical results simulated by the Isopro 3.0 program. The results indicate that the metal-ligated skeleton of CTB is stable while the bromide ligand is labile in solution, suggesting that the neutral copper center could become positively charged after losing Br^- , which may facilitate CTB to interact with DNA or target at mitochondria.

Cellular and mitochondrial uptake

The cellular copper content in MCF-7, HeLa, Skov-3, A549 and A549R tumor cells was tested by ICP-MS. The copper uptake capability of these cells differs significantly with each other, for instance, that of MCF-7 cells is nearly 4 times greater than that of Skov-3 cells. The detailed data for each cell line are listed in Table 4. The results suggest that CTB could pass through the membrane of these cells and accumulate in the cytoplasm, whereupon it may further enter into the mitochondrion and even nucleus to exert the biological effects. MCF-7, A549R and A549 cell lines seem to be more vulnerable to the attack of CTB than

Table 5 The content of Cu in 10^6 HeLa cells and their mitochondria. The values were calculated according to the data of at least three independent replicates and expressed in mass (ng) and density ($\text{ng}\mu\text{L}^{-1}$).

Complex	Cu in cells		Cu in mitochondria	
	mass	density	mass	density
Blank	2.61 ± 0.87	0.13	0.08 ± 0.02	0.02
CTB ^a	49.12 ± 2.97	3.07	9.77 ± 1.02	3.26
$[\text{Cu}(\text{tpp})\text{Br}_2]^a$	56.77 ± 4.45	3.34	4.89 ± 0.52	1.63

^aBlank value has been subtracted from the total amount.

HeLa and Skov-3 cell lines, which are expected to result in different cellular consequences.

The mitochondrial uptake of CTB was examined by two methods. Firstly, ICP-MS was used to determine the copper content in HeLa cells and their mitochondria. In order to ascertain whether CTB possesses any mitochondrion-targeting property, $[\text{Cu}(\text{tpp})\text{Br}_2]$, an analogue of CTB without the targeting TPP group, was used as a reference. The results listed in Table 5 indicate that both CTB and $[\text{Cu}(\text{tpp})\text{Br}_2]$ can pass through the membrane of the cells and mitochondria. For CTB, the copper density in mitochondria and cells is 3.26 and $3.07 \text{ ng}\mu\text{L}^{-1}$ respectively, displaying some targeting propensity for mitochondria. Furthermore, the copper content and density in the mitochondria are higher for CTB (9.77 ng and $3.26 \text{ ng}\mu\text{L}^{-1}$) than for $[\text{Cu}(\text{tpp})\text{Br}_2]$ (4.89 ng and $1.63 \text{ ng}\mu\text{L}^{-1}$), indicating the former has a salient affinity for mitochondria. Considering the copper content and density in the mitochondria of untreated cells are extremely low, the seemingly insignificant increase in mitochondrial uptake for CTB is actually quite noteworthy.

Secondly, fluorescence spectrometry was used to test the relative content of CTB in Skov-3 cells and their mitochondria after CTB was incubated with the cells for 48 h. As Fig. 4 shows, CTB has a characteristic emission peak at 546 nm ($\lambda_{\text{ex}} = 460 \text{ nm}$) in cell-free aqueous solution. The mitochondrial lysis solution and the cellular digestion liquid with the same volume also exhibit emission peaks at 546 nm , which indicates that CTB can penetrate the cellular and mitochondrial membranes of Skov-3 cells. Plainly, the fluorescence intensity of the mitochondrial solution is higher than that of the cellular liquid, suggesting that the concentration of CTB in mitochondria exceeds that in cells. The results of above two experiments demonstrate that CTB is able to target the mitochondria of HeLa and Skov-3 cells, even though their cellular content of copper is relatively low among the tested tumor cell lines (Table 4). Apparently, the preferential accumulation of CTB in mitochondria results from the TPP targeting group.

Lipophilicity and electric charge

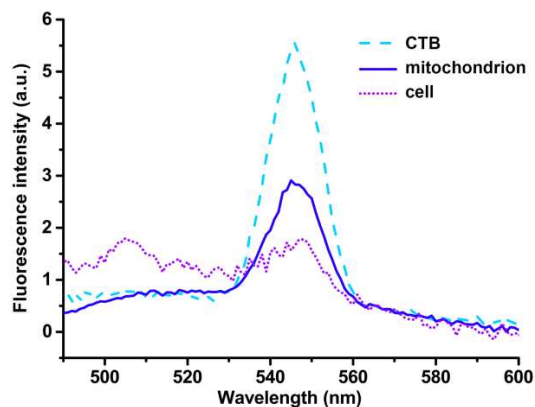


Fig. 4 The fluorescence spectra of CTB ($\lambda_{\text{ex}} = 460$ nm) in cell-free aqueous solution ($0.1 \mu\text{M}$), in mitochondrial lysis solution, or in cellular digestion solution with the same volume after cultivating CTB ($2 \mu\text{M}$) with Skov-3 cells in RPMI-1640 medium for 48 h.

Table 6 The UV absorbance of CTB in phosphate buffer and 1-octanol at different concentrations and the corresponding lipophilicity.

CTB (μM)	$\text{Ab}_{\text{buffer}}$		$\text{Ab}_{\text{octanol}}$	$\text{Log } P_{\text{o/w}}$
	before shake	after shake		
50	1.872	1.328	0.544	-0.387
100	3.332	2.382	0.950	-0.399
200	6.248	4.450	1.798	-0.394

The cellular uptake and tumor selectivity of CTB could be affected by several factors such as lipophilicity of the complex and membrane potentials ($\Delta\Psi$) of the tumor cells. The lipophilicity of CTB was determined with the established shake-flask method in a 1-octanol/phosphate buffer system (pH 7.4). The lipo-hydro partition coefficients ($\text{Log } P_{\text{o/w}}$) calculated under different CTB concentrations are listed in Table 6. The negative average $\text{Log } P$ value (-0.39) means that CTB is a hydrophilic compound. It is known that hydrophilic cationic compounds with slow diffusion kinetics ($\text{Log } P = 0$ to -3.0) preferentially accumulate in tumor cells or tissues,²⁷ therefore, CTB may have a high selectivity for tumor cells.

In general, charged molecules cannot traverse cell membranes without the aid of transporter proteins owing to the large activation energies related with the removal of associated water molecules. The data in Tables 4 and 5, however, demonstrate that the electric charge did not prevent CTB from penetrating the cellular and mitochondrial membranes. This may be due to the distribution of charge across the large lipophilic surface of the phosphonium ion significantly lowers the energy requirement and thereby facilitates the passage through lipid membranes.²⁶ On the other hand, the high plasma membrane potential $\Delta\Psi_p$ (30–60 mV, negative inside) can pre-concentrate the cationic species and thus enhance their cytoplasmic concentration and availability for mitochondrial uptake.²³ Additionally, the difference in $\Delta\Psi_m$ between cancer cells and normal epithelial cells is about 60 mV (negative inside), which could result in a 10-fold greater accumulation of cationic compounds in mitochondria of cancer cells.¹⁹ In brief, both the positive charge and low lipophilicity of CTB are responsible for its accumulation in cancer cells. Of course, besides the passive transport, other channels such as the copper transport protein pathway might also play a role in penetrating the cell membranes.^{30,31}

Dissipation of the mitochondrial membrane potential

Dissipation of $\Delta\Psi_m$ before, during, or after the mitochondrial outer membrane permeabilization is the hallmark of apoptosis proceeding through the mitochondrial pathway.³² The dissipation of $\Delta\Psi_m$ could be detected by fluorescence probe 5,5',6,6'-tetrachloro-1,1',3,3'-tetraethylbenzimidazolylcarbocyanine iodide (JC-1), which aggregates in the mitochondrial matrix and emits red fluorescence as mitochondria are intact with normal $\Delta\Psi_m$, while remains as a monomer and emits green fluorescence as mitochondria are depolarized with abnormal $\Delta\Psi_m$.³³ Therefore, a concentration-dependent shift from red to green in the emission spectrum of JC-1 measured by flow cytometry can be interpreted as an indication of $\Delta\Psi_m$ dissipation.³⁴ A representative flow cytometric plot reflecting the effects of CTB or cisplatin on HeLa cells after incubation for 48 h with JC-1 is shown in Fig. S1 (see ESI†). The corresponding impacts on the emission spectrum of JC-1 are shown in Fig. 5. A mitochondrial metabolic inhibitor carbonyl cyanide *m*-chlorophenyl hydrazone (CCCP) is used as a positive contrast, which is capable of inducing the dissipation of $\Delta\Psi_m$.^{35,36} The changes of the red fluorescence intensity ($\lambda_{\text{em}} = 590$ nm) are presented to show the red-to-green fluorescence shift. The fluorescence of the control is quite strong (10^3), suggesting mitochondria are unimpaired and $\Delta\Psi_m$ is normal; while that in the presence of CCCP is much weak (10^2), suggesting mitochondria are impaired and $\Delta\Psi_m$ is dissipated. In comparison with the control, CTB can exert a manifest influence on the mitochondria even at low concentrations (1–2 μM), in that the fluorescence intensity of considerable amount of cells decreases to the low level (10^2). Cisplatin, however, only displays a moderate influence on the mitochondria at a relatively high concentration (4 μM). The results indicate that CTB is a more effective stimulator than cisplatin for the dissipation of $\Delta\Psi_m$, which may be attributed to the contribution of the mitochondrion-targeting moiety TPP.

Cytotoxicity

The cytotoxicity of CTB against the human breast carcinoma MCF-7, the human cervical cancer HeLa, and the human ovarian cancer Skov-3 cell lines was first tested by the MTT [3-(4,5-dimethylthiazol-2-yl)-2,5-diphenyltetrazolium bromide] assay, using cisplatin as the control. As Fig. 6A shows, CTB is more cytotoxic against these cell lines than cisplatin. For example, the inhibition rate of CTB for MCF-7 cells is 57.9% at 1 μM , while that of cisplatin is far below 10% at the same concentration. The IC_{50} values of CTB for these cell lines range from 0.87 to 6.80 μM (Table 7). The cytotoxicity was further tested on the human lung adenocarcinoma A549 and its cisplatin-resistant A549R cell lines. As shown in Fig. 6B, CTB displays a significant inhibition activity towards these cancer cells. For example, the inhibition rate of CTB is 95.6% for A549 cells and 97.7% for A549R cells at 20 μM ; even at 1 μM , the inhibition rate still reaches 51.0% for A549 cells and 44.8% for A549R cells. Apparently, the inhibition efficacy of CTB is much higher than that of cisplatin, especially at low concentrations ($< 10 \mu\text{M}$). The IC_{50} values for A549 and A549R cells are 1.01 and 1.54 μM (Table 7), respectively. The resistance factor (RF) is 1.52, which is defined as the ratio between the IC_{50} value for the resistant cells and that for the sensitive ones.³⁷ This certifies that the cytotoxicity of CTB

towards A549 and A549R cells is very similar, and A549R cells do not show evident resistance to CTB. By contrast, the resistance of A549R cells to cisplatin is marked at low

concentrations. The results indicate that CTB has the potential to circumvent the drug resistance to cisplatin.

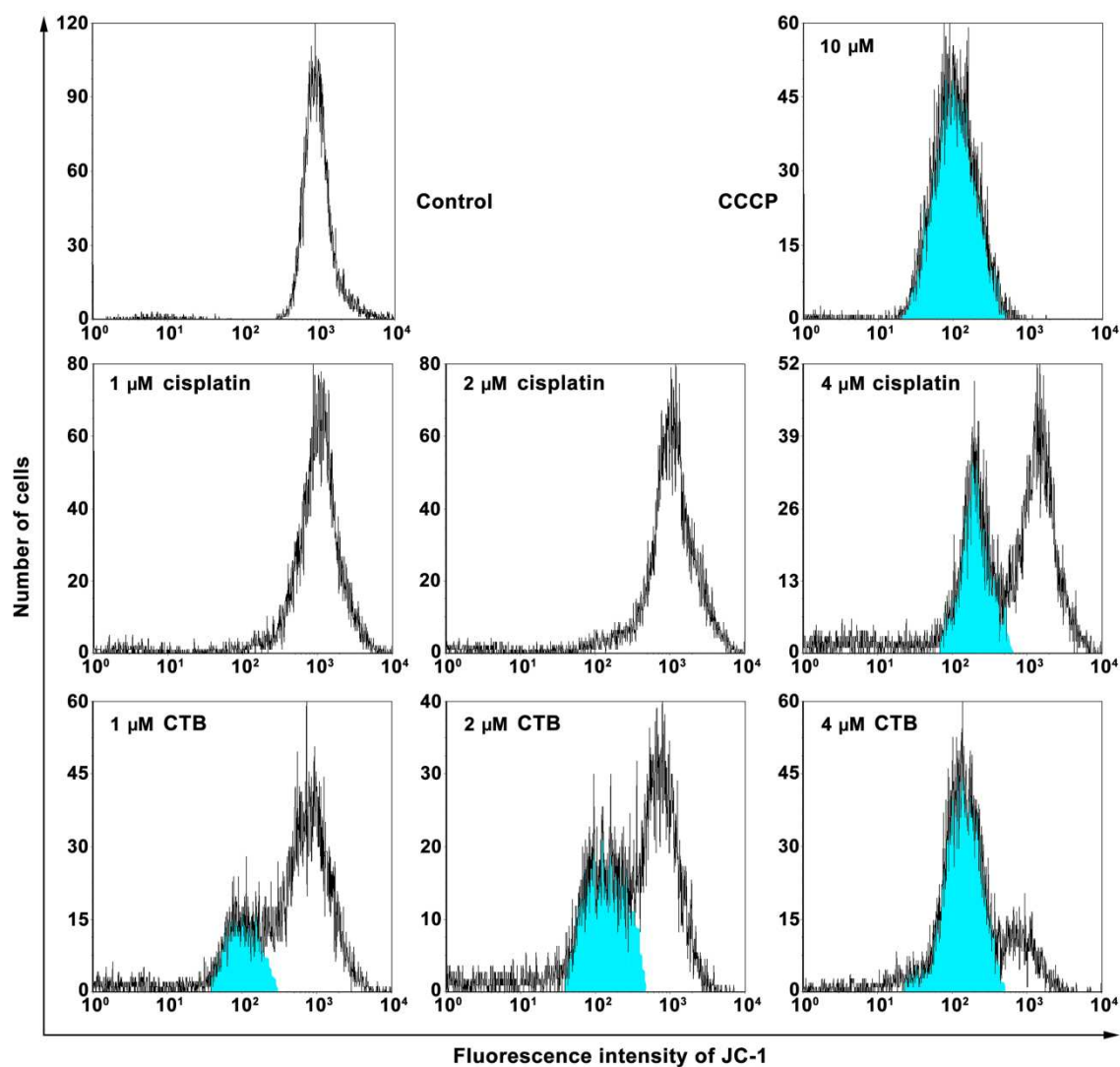


Fig. 5 The impacts of CTB or cisplatin on the red fluorescence intensity ($\lambda_{em} = 590$ nm) of JC-1 after incubation with HeLa cells for 48 h determined by flow cytometry.

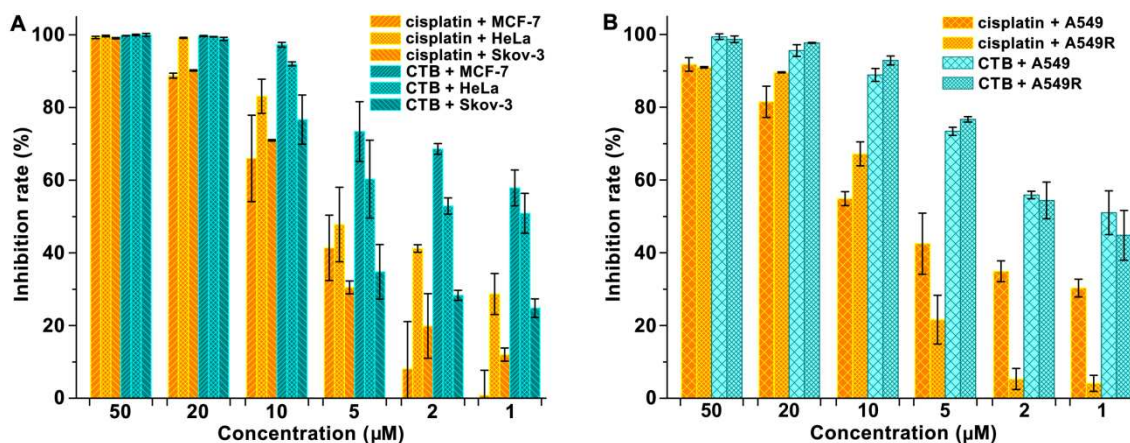


Fig. 6 Cytotoxicity of CTB against MCF-7, HeLa, Skov-3, A549, and A549R cell lines (48 h) at different concentrations (50, 20, 10, 5, 2, 1 μ M), with cisplatin as the reference. Data are presented as the mean \pm SD of three independent experiments.

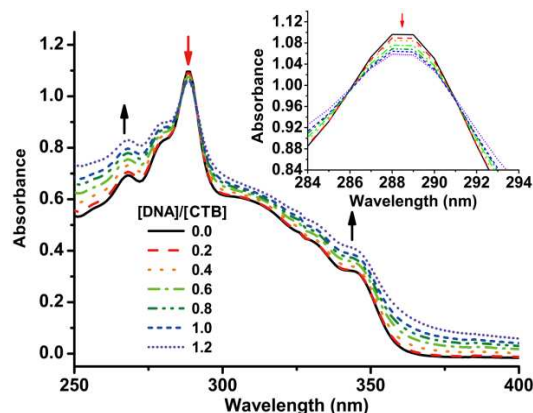


Fig. 7 UV spectra of CTB (15 μM) in the absence and presence of CT-DNA with $[\text{DNA}]/[\text{CTB}]$ ratios increasing from 0 to 1.2 in the buffer (5 mM Tris-HCl/50 mM NaCl, pH 7.4).

Table 7 IC_{50} values (μM) of CTB and cisplatin for MCF-7, HeLa, Skov-3, A549 and A549R cell lines at 48 h.

Complex	MCF-7	HeLa	Skov-3	A549	A549R
CTB	0.87	0.95	6.80	1.01	1.54
cisplatin	6.46	5.25	7.08	7.58	8.91

Interestingly, the cytotoxicity of CTB is positively related to the cellular uptake of Cu (see Table 4), that is, the most sensitive tumor cells are just those that take in the largest amount of Cu and vice versa. The correlation between the cytotoxicity and the uptake of Cu suggests that the metal plays some crucial roles in the cytostatic mechanism of CTB, which is confirmed by the following experiments.

15 DNA binding properties

To elucidate the possible mechanism of action behind the cytotoxic activity of the complex, the interaction between CTB and CT-DNA was first studied by UV spectroscopy. The UV spectrum of CTB in the buffer shows an intense band at 288 nm (Fig. 7), which could be assigned to the intra ligand transitions of ttpy-tpy.³⁸ Upon addition of increasing concentrations of CT-DNA to the solution of CTB, a hypochromism is observed at 288 nm, which is one of the most immediate indications of possible intercalative binding to DNA.³⁹ The planarity and extended aromaticity of the terpyridine system are favourable for the stacking of CTB between the DNA base pairs.

Since ttpy-tpy is a cationic ligand and the copper center could become positively charged in solution, whereas the phosphate backbone of DNA is negatively charged, the interaction between CTB and DNA could be stabilized through electrostatic interactions. This was testified by the UV titration in the buffer solution with increasing concentration of NaCl. As Fig. 8 shows, in a fixed $[\text{DNA}]/[\text{CTB}]$ ratio (0.4), the UV spectra of CTB change apparently with the variation of NaCl concentrations. As NaCl is below 50 mM, the absorbance at 288 nm increases with the augment of NaCl, suggesting the interaction between CTB and DNA is weakened. This is because Na^+ could compete with CTB cations for neutralizing the DNA phosphates and hence screen more CTB cations from the interaction. As NaCl is above 50 mM, the influence of Cl^- on CTB cations becomes apparent and thus a hypochromism positively related to the concentration

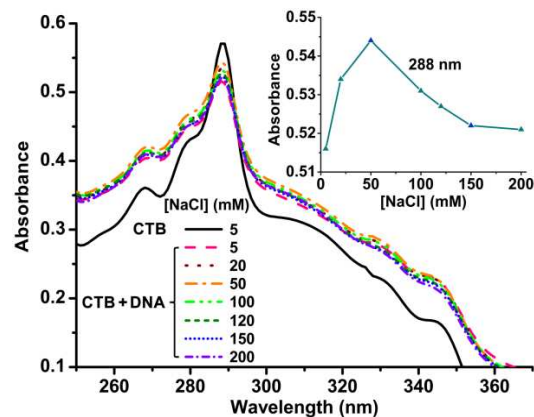


Fig. 8 UV spectra of CTB (15 μM) in the absence and presence of CT-DNA ($[\text{DNA}]/[\text{CTB}] = 0.4$) in the buffer (5 mM Tris-HCl/NaCl, pH 7.4) with increasing amounts of NaCl (5–200 mM). Inset shows the UV absorption of CTB versus the NaCl concentrations at 288 nm.

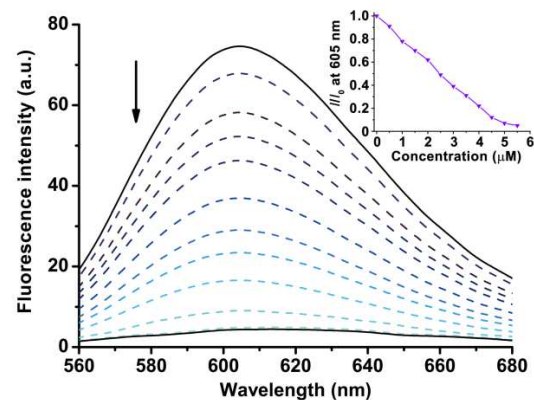


Fig. 9 Emission profiles ($\lambda_{\text{ex}} = 526 \text{ nm}$) of the EB-DNA system in the buffer (5 mM Tris-HCl/50 mM NaCl, pH 7.4) upon addition of CTB (0–5.5 μM) at 25 $^{\circ}\text{C}$.

Of NaCl appears. As NaCl is beyond 150 mM, all the electrostatic interactions have reached equilibrium and therefore the absorbance of CTB becomes steady. These spectroscopic changes suggest that NaCl could weaken the intercalation between CTB and DNA through non-specific electrostatic interactions. Thus, electrostatic interaction is a major factor contributing to the interaction between CTB and DNA.

The DNA binding behavior of CTB was further investigated using the EB-DNA system. This system generally gives a significant increase in the fluorescence emission when intercalator ethidium bromide (EB) is bound to DNA, and a decrease in the fluorescence when EB is displaced.⁴⁰ As Fig. 9 shows, the fluorescence intensity (I) of the EB-DNA system at 605 nm decreases until nearly to 0 with the titration of CTB from 0 to 5.5 μM , suggesting that CTB can replace the DNA-bound EB through an intercalative interaction. According to the titration profile, the apparent binding constant K_{app} of CTB to DNA was calculated to be $4.05 \times 10^6 \text{ M}^{-1}$.⁴¹

The conformational changes of DNA induced by CTB were investigated by CD spectroscopy. The CD spectra of CT-DNA before and after the addition of different concentrations of CTB are shown in Fig. 10. The positive band at about 278 nm is due to the base stacking and the negative band at about 248 nm is due to

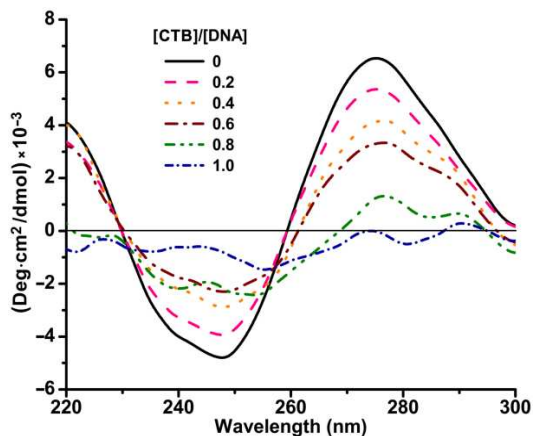


Fig. 10 CD spectra of CT-DNA (0.1 mM) in the absence and presence of CTB in different [CTB]/[DNA] ratios.

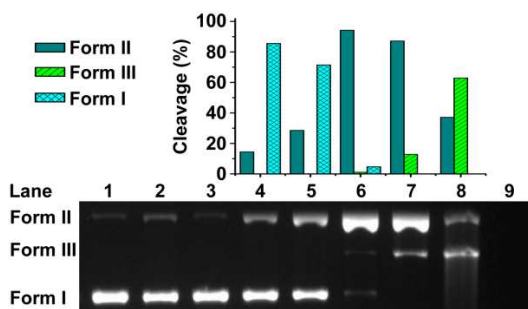


Fig. 11 The cleavage patterns of the agarose gel electrophoresis and the corresponding cleavage extent (%) for pBR322 plasmid DNA (200 ng) by CTB and Vc (1 mM) in the buffer solution (50 mM Tris-HCl/50 mM NaCl, pH 7.4) at 37 °C for 60 min. Lane 1, DNA control; lane 2, DNA + Vc; lane 3, DNA + CTB (12 μ M); lanes 4–9, DNA + Vc + CTB (2, 4, 6, 8, 10, 12 μ M, respectively).

the helicity, which are the characteristics of B-DNA.⁴² In the presence of CTB, both the positive and negative bands decrease markedly in ellipticity, and the bands become nearly flat when the ratio of [CTB]/[DNA] increases to 1.0, suggesting that CTB can unwind the DNA helix and lead to the loss of helicity.⁴³ The UV, fluorescence and CD results indicate that CTB can strongly interact with DNA through an intercalative mode driven by the electrostatic force between CTB cations and DNA phosphate anions. These interactions are supposed to elicit effective cleavage activity towards DNA and strong cytotoxicity against cancer cells.

DNA cleavage activity

The DNA cleavage activity of CTB was studied using supercoiled pBR322 plasmid DNA in the presence of ascorbic acid (Vc) by agarose gel electrophoresis in the buffer. As Fig. 11 shows, CTB can convert Form I DNA into Form II at 2 μ M (lane 4), and can completely cleave Form I DNA into Form II (87.2%) and Form III DNA (12.8%) at 8 μ M (lane 7). Linear DNA (Form III) appears at 6 μ M (1.1%) (lane 6), and increases to 62.9% at 10 μ M (lane 8). Form I DNA is totally cut up at 12 μ M (lane 9). The results demonstrate that CTB has a remarkable DNA cleavage activity in the presence of Vc. Just as the cytotoxicity, the DNA cleavage activity of CTB is also positively related to its concentration, which may imply that cleavage of DNA plays an important part in the cytostatic mechanism of CTB.

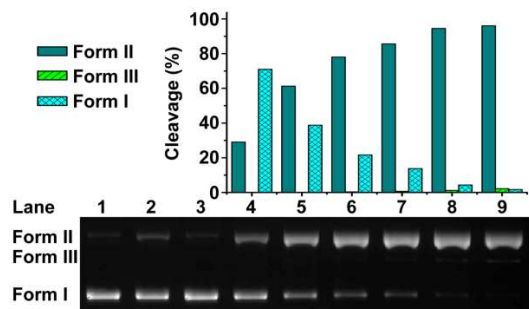


Fig. 12 The time-dependent cleavage patterns of the agarose gel electrophoresis and the corresponding cleavage extent (%) for pBR322 plasmid DNA (200 ng) by CTB (4 μ M) and Vc (1 mM) in the buffer solution (50 mM Tris-HCl/50 mM NaCl, pH 7.4) at 37 °C. Lanes 1–3, DNA, DNA + Vc, and DNA + CTB at 90 min, respectively; lanes 4–9, DNA + Vc + CTB at 15, 30, 45, 60, 75, and 90 min, respectively.

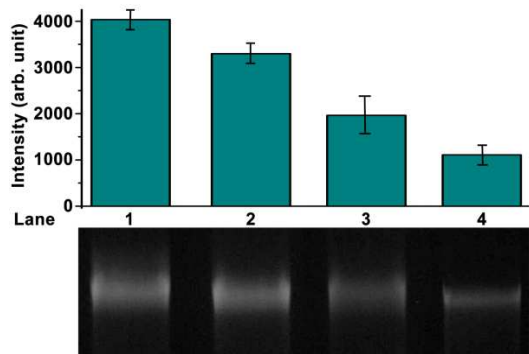


Fig. 13 The cleavage patterns of the agarose gel electrophoresis and the relative intensity of each band for DNA (20 ng μ L⁻¹) isolated from HeLa cells after cultivation in the buffer solution (50 mM Tris-HCl/50 mM NaCl, pH 7.4) at 37 °C for 60 min. Lane 1, medium + 10% FBS; lane 2, medium + 10% FBS + Vc (1 mM); lane 3, medium + 10% FBS + CTB (2 μ M); lane 4, medium + 10% FBS + CTB (2 μ M) + Vc (1 mM).

The time-dependent cleavage of pBR322 DNA mediated by CTB (4 μ M) was followed with agarose gel electrophoresis in the buffer at 37 °C. As shown in Fig. 12, in the whole time course (15–90 min), Form II DNA displays an ever-increasing trend, in that it changes from 29.1% to 96.1%. Both the concentration- and time-dependent data lead to the same conclusion that CTB can efficiently cleave DNA, which forms the basis for its cytotoxic activity.

The DNA cleavage activity of CTB was further tested on intracellular DNA isolated from HeLa cells after cultivation for 48 h. Fig. 13 shows the gel electrophoresis results of the DNA cleavage test in different conditions. All lanes show a single band with different intensities. The cleavage activity was estimated on the DNA contents calculated by Quantity One Software. In comparison with the control (lane 1), CTB can cleave 50% of DNA at 2 μ M (lane 3); in the presence of Vc, it can cleave nearly 75% of DNA at the same concentration (lane 4). The results demonstrate that CTB also possesses a remarkable cleavage activity for intracellular DNA of cancer cells even in the absence of extrinsic Vc.

Identification of ROS

The potential ROS responsible for the DNA cleavage were identified using common radical scavengers such as DMSO, KI, NaN₃ and D₂O, respectively. As Fig. 14 presents, the cleavage

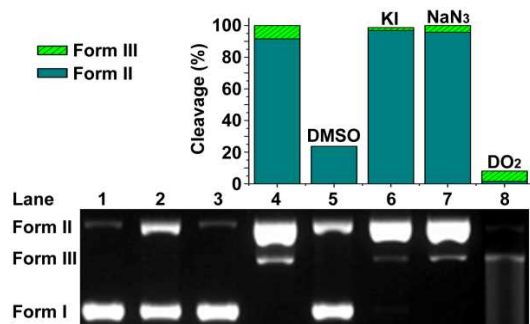


Fig. 14 The cleavage patterns of the agarose gel electrophoresis for pBR322 plasmid DNA (200 ng) by CTB (4 μ M) and the corresponding cleavage efficiency in the presence of Vc (1 mM) after incubation without or with different radical scavengers at 37 $^{\circ}$ C for 1 h. Lane 1, DNA control; lane 2, DNA + Vc; lane 3, DNA + CTB; lane 4, DNA + CTB + Vc; lanes 5–8, DNA + CTB + Vc + S, S stands for DMSO (10%), KI (10 mM), NaN_3 (10 mM) and D_2O (70%), sequentially.

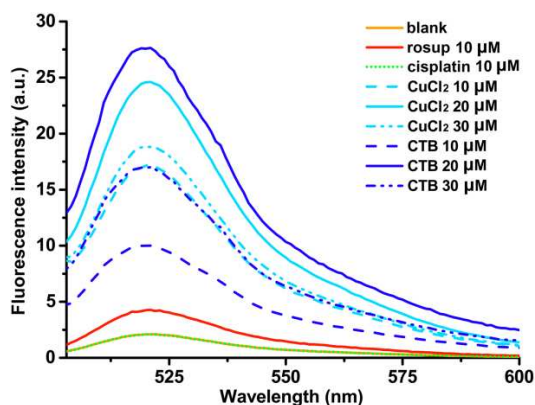


Fig. 15 The fluorescence intensity of DCF ($\lambda_{\text{ex}} = 488$ nm) induced by different concentrations of CTB, CuCl_2 and cisplatin, respectively, in HeLa cells at 37 $^{\circ}$ C for 1 h, with rosup as a positive control.

activity of CTB is reduced dramatically in the presence of hydroxyl radical scavenger DMSO (lane 5), indicating that diffusible $\cdot\text{OH}$ plays a key role in the cleavage process. Hydrogen peroxide scavenger KI (lane 6) and singlet oxygen scavenger NaN_3 (lane 7) hardly influence the cleavage, suggesting that H_2O_2 and $^1\text{O}_2$ are barely involved in the cleavage mechanism. The cleavage activity of CTB in D_2O , where the lifetime of $^1\text{O}_2$ is significantly longer than that in water, further demonstrates their irrelevance of $^1\text{O}_2$ to the cleavage (lane 8). The results indicate that hydroxyl radicals are the crucial ROS responsible for the cleavage activity of CTB.

The ROS generated in cancer cells were detected using a fluorescence probe 2',7'-dichlorofluorescein diacetate (DCFH-DA), which could easily penetrate cell membrane and be hydrolyzed by intracellular esterase to form DCFH. DCFH has no fluorescence and cannot pass through the cell membrane, so it could be easily enriched in cells. Since ROS produced in cells could oxidize DCFH into fluorescent 2',7'-dichlorofluorescein (DCF), thus the fluorescence intensity of DCF can indicate the level of intracellular ROS.⁴⁴ The fluorescence of the cell suspensions was determined after HeLa cells were cultured with CTB, CuCl_2 or cisplatin for 1 h, using rosup as a positive reference. As Fig. 15 shows, CTB and CuCl_2 can significantly enhance the fluorescence intensity at different concentrations, while cisplatin can hardly influence the fluorescence. The effect

of CTB seems to be more dependent on the concentration as compared with that of the simple salt CuCl_2 ; however, the variation tendencies are the same, indicating that in both cases Cu^{II} is involved in the generation of ROS. According to the redox potential of CTB (Fig. S2, see ESI[†]), the reduction of Cu^{II} to Cu^{I} may be mediated by the intracellular reducing agents such as glutathione.⁴⁵ Anyway, the results suggest that CTB is an effective ROS inducer and is likely to exert some effects on cancer cells dissimilar from those yielded by cisplatin.

On the basis of above facts, we believe that the cytostatic activity of CTB mainly arises from the following molecular events. Firstly, the strong binding of CTB to DNA through both intercalative and electrostatic interactions could unwind the DNA helix and block up the DNA replication; secondly, the efficient cutting of DNA by CTB through an oxidative pathway could utterly damage the cellular DNA strands and make the DNA repair mechanism of tumor cells fail to take effect. Nevertheless, tumor cells typically exhibit higher ROS levels in comparison with normal cells, so that even a minor increase of ROS in tumor mitochondria might be sufficient to push total ROS levels beyond the critical threshold and lead to apoptosis.^{46,47,48} Therefore, ROS may be implicated in the mechanism of action more deeply than we presumed here. Undoubtedly, the underlying molecular basis for the cytotoxicity of CTB remains to be defined further.

Conclusions

Various side effects of platinum anticancer drugs are chiefly due to their lack of specificity for tumor cells. The differences in plasma and/or mitochondrial membrane potentials between normal and tumor cells provide an opportunity to design drugs with preferential selectivity for tumor cells. In this study, a mitochondrion-targeting group TPP was introduced into the copper-terpyridine complex to enhance its selectivity and cytostatic activity for tumor cells. TPP helps the complex penetrate cellular and mitochondrial membranes and target at mitochondria, while the copper center exerts the inhibitory effect via an oxidative mechanism. We demonstrated that the copper complex can inhibit cancer cells through multiple pathways, including the structural modification of DNA, production of ROS, scission of DNA strands, and dissipation of $\Delta\Psi_{\text{m}}$. This study provides a unique example for the rational design of copper complexes as potential anticancer drugs. The encouraging results make us believe that copper complexes with mitochondrion-targeting potential could bring about anticancer efficacy unreachable for platinum drugs.

Acknowledgements

We are grateful to the National Natural Science Foundation of China (Grants 21271101, 21131003, 21021062, 91213305) and the National Basic Research Program of China (Grant 2011CB935800) for the financial support.

Notes and references

^aState Key Laboratory of Coordination Chemistry, School of Chemistry and Chemical Engineering, Nanjing University, Nanjing 210093, P. R. China. Fax: +862583314502; Tel: +86 25 83594549; E-mail: zguo@nju.edu.cn

^bState Key Laboratory of Pharmaceutical Biotechnology, School of Life Sciences, Nanjing University; State Key Laboratory of Analytical Chemistry for Life Science, Nanjing University, Nanjing 210093, P. R. China. Fax: +862583314502; Tel: +86 25 83594549; E-mail: boxwxy@nju.edu.cn

† Electronic Supplementary Information (ESI) available: detailed experimental procedures, supplementary results and figures. See DOI: 10.1039/b000000x/

- 1 N. P. Farrell, *Curr. Top. Med. Chem.*, 2011, **11**, 2623–2631.
- 2 X. Y. Wang, *Anti-Cancer Agents Med. Chem.*, 2010, **10**, 396–411.
- 3 X. Y. Wang and Z. J. Guo, *Dalton Trans.*, 2008, 1521–1532.
- 4 P. Heffeter, U. Jungwirth, M. Jakupec, C. Hartinger, M. Galanski, L. Elbling, M. Micksche, B. Keppler and W. Berger, *Drug Resist. Updates*, 2008, **11**, 1–16.
- 5 X. Y. Wang and Z. J. Guo, *New Trends and Future Developments of Platinum-Based Antitumor Drugs*, in: E. Alessio (Ed.), *Bioinorganic Medicinal Chemistry*, WILEY-VCH Verlag GmbH & Co. KGaA, Weinheim, 2011, pp. 97–149.
- 6 L. Kelland, *Nat. Rev. Cancer*, 2007, **7**, 573–584.
- 7 L. P. Martin, T. C. Hamilton and R. J. Schilder, *Clin. Cancer Res.*, 2008, **14**, 1291–1295.
- 8 S. Komeda and A. Casini, *Curr. Top. Med. Chem.*, 2012, **12**, 219–235.
- 9 K. J. Kilpin and P. J. Dyson, *Chem. Sci.*, 2013, **4**, 1410–1419.
- 10 C. Marzano, M. Pellei, F. Tisato and C. Santini, *Anti-Cancer Agents Med. Chem.*, 2009, **9**, 185–211.
- 11 D. Palanimuthu, S. V. Shinde, K. Somasundaram and A. G. Samuelson, *J. Med. Chem.*, 2013, **56**, 722–734.
- 12 S. Tardito, A. Barilli, I. Bassanetti, M. Tegoni, O. Bussolati, R. Franchi-Gazzola, C. Mucchio and L. Marchiò, *J. Med. Chem.*, 2012, **55**, 10448–10459.
- 13 M. J. Burkitt, *Methods Enzymol.*, 1994, **234**, 66–79.
- 14 F. Tisato, C. Marzano, M. Porcchia, M. Pellei and C. Santini, *Med. Res. Rev.*, 2010, **30**, 708–749.
- 15 C. Santini, M. Pellei, V. Gandin, M. Porchia, F. Tisato and C. Marzano, *Chem. Rev.*, 2014, **114**, 815–862.
- 16 Z. Zhang, C. Bi, S. M. Schmitt, Y. Fan, L. Dong, J. Zuo and Q. P. Dou, *J. Biol. Inorg. Chem.*, 2012, **17**, 1257–1267.
- 17 D. Pathania, M. Millard and N. Neamati, *Adv. Drug Deliv. Rev.*, 2009, **61**, 1250–1275.
- 18 G. Kroemer, L. Galluzzi and C. Brenner, *Physiol. Rev.*, 2007, **87**, 99–163.
- 19 J. S. Modica-Napolitano and J. R. Aprile, *Adv. Drug Deliv. Rev.*, 2001, **49**, 63–70.
- 20 J. S. Armstrong, *Br. J. Pharmacol.*, 2007, **151**, 1154–1165.
- 21 M. D. Siegelin, T. Dohi, C. M. Raskett, G. M. Orłowski, C. M. Powers, C. A. Gilbert, A. H. Ross, J. Plescia and D. C. Altieri, *J. Clin. Invest.*, 2011, **121**, 1349–1360.
- 22 C. Yan, J. S. Oh, S. H. Yoo, J. S. Lee, Y. G. Yoon, Y. J. Oh, M. S. Jang, S. Y. Lee, J. Yang, S. H. Lee, H. Y. Kim and Y. H. Yoo, *Toxicol. Appl. Pharm.*, 2013, **266**, 9–18.
- 23 M. P. Murphy, *Biochim. Biophys. Acta*, 2008, **1777**, 1028–1031.
- 24 R. J. Dubois, C. -C. L. Lin and J. A. Beisler, *J. Med. Chem.*, 1978, **21**, 303–306.
- 25 K. L. Bergeron, E. L. Murphy, O. Majofodun, L. D. Muñoz, J. C. Williams Jr and K. H. Almeida, *Mutat. Res. Genet. Toxicol. Environ. Mutagen.*, 2009, **673**, 141–148.
- 26 M. Millard, D. Pathania, Y. Shabaik, L. Taheri, J. Deng and N. Neamati, *PLoS ONE*, 2010, **5**, e13131.
- 27 J. Wang, C. -T. Yang, Y. -S. Kim, S. G. Sreerama, Q. Cao, Z. -B. Li, Z. He, X. Chen and S. Liu, *J. Med. Chem.*, 2007, **50**, 5057–5069.
- 28 Y. -S. Kim, C. -T. Yang, J. Wang, L. Wang, Z. -B. Li, X. Chen and S. Liu, *J. Med. Chem.*, 2008, **51**, 2971–2984.
- 29 W. Zhou, X. Y. Wang, M. Hu and Z. J. Guo, *J. Inorg. Biochem.*, 2013, **121**, 114–120.
- 30 S. Puig, J. Lee, M. Lau and D. J. Thiele, *J. Biol. Chem.*, 2002, **277**, 26021–26030.
- 31 P. V. E. van den Berghe and L. W. J. Klomp, *J. Biol. Inorg. Chem.*, 2010, **15**, 37–46.
- 32 D. R. Green and G. Kroemer, *Science*, 2004, **305**, 626–629.
- 33 S. T. Smiley, M. Reers, C. Mottola-Hartshorn, M. Lin, A. Chen, T. W. Smith, G. D. Steele, Jr. and L. B. Chen, *Proc. Natl. Acad. Sci. USA*, 1991, **88**, 3671–3675.
- 34 G. Kroemer and J. C. Reed, *Nat. Med.*, 2000, **6**, 513–519.
- 35 G. Biswas, O. A. Adebajo, B. D. Freedman, H. K. Anandatheerthavarada, C. Vijayarathy, M. Zaidi, M. Kotlikoff and N. G. Avadhani, *EMBO J.*, 1999, **18**, 522–533.
- 36 M. Reers, T. W. Smith and L. B. Chen, *Biochemistry*, 1991, **30**, 4480–4486.
- 37 N. Margiotta, R. Ostuni, V. Gandin, C. Marzano, S. Piccinonna and G. Natile, *Dalton Trans.*, 2009, 10904–10913.
- 38 V. M. Manikandamathavan, R. P. Parameswari, T. Weyhermüller, H. R. Vasanthi and B. U. Nair, *Eur. J. Med. Chem.*, 2011, **46**, 4537–4547.
- 39 S. A. Tysse, R. J. Morgan, A. D. Baker and T. C. Strekas, *J. Phys. Chem.*, 1993, **97**, 1707–1711.
- 40 J. B. LePecq and C. Paoletti, *J. Mol. Biol.*, 1967, **27**, 87–106.
- 41 M. Lee, A. L. Rhodes, M. D. Wyatt, S. Forrow and J. A. Hartley, *Biochemistry*, 1993, **32**, 4237–4245.
- 42 W. C. Johnson, in: K. Nakanishi, N. Berova and R. W. Woody (Eds.), *Circular Dichroism: Principles and Applications*, VCH, New York, 1994, 523–540.
- 43 K. Karidi, A. Garoufīs, N. Hadjiliadis and J. Reedijk, *Dalton Trans.*, 2005, 728–734.
- 44 W. O. Carter, P. K. Narayanan and J. P. Robinson, *J. Leukoc. Biol.*, 1994, **55**, 253–258.
- 45 C. R. Kowol, P. Heffeter, W. Miklos, L. Gille, R. Trondl, L. Cappellacci, W. Berger and B. K. Keppler, *J. Biol. Inorg. Chem.*, 2012, **17**, 409–423.
- 46 D. Trachootham, J. Alexandre and P. Huang, *Nat. Rev. Drug Discovery*, 2009, **8**, 579–591.
- 47 A. Gupte and R. J. Mumper, *Cancer Treat. Rev.*, 2009, **35**, 32–46.
- 48 M. Nagai, N. H. Vo, L. S. Ogawa, D. Chimmanamada, T. Inoue, J. Chu, B. C. Beaudette-Zlatanova, R. Lu, R. K. Blackman, J. Barsoum, K. Koya and Y. Wada, *Free Radic. Biol. Med.*, 2012, **52**, 2142–2150.